KSCE Journal of Civil Engineering (2022) 26(8):3301-3313
DOI 10.1007/s12205-022-1308-6

pISSN 1226-7988, eISSN 1976-3808
www.springer.com/12205

Geotechnical Engineering

Stability Analysis of Subgrade under Dynamic Loading of Single and Double High-Speed Railways in Karst Areas

Pengxiang Li[a], **Mingzhou Bai**[a,b], **Zijun Wei**[a], **Xin Li**[a], **and Hai Shi**[a]

[a]*School of Civil Engineering, Beijing Jiaotong University, Beijing 100044, China*
[b]*Beijing Key Laboratory of Track Engineering, Beijing Jiaotong University, Beijing 100044, China*

ARTICLE HISTORY

Received 20 July 2021
Revised 12 November 2021
Accepted 24 February 2022
Published Online 31 May 2022

KEYWORDS

Karst hole
Single and double railways
Vibration wave
Subgrade stability
Dynamic response
Sinkholes

ABSTRACT

With the increase in the use of high-speed trains, karst collapse disasters have become increasingly prominent during the construction and operation of railway projects. To study the propagation characteristics of vibration wave caused by single and double railways in karst area, as well as the influence of sinkholes on the stability of the roadbed, a coupling model of vehicle-track-subgrade (including underlying sinkhole) considering track irregularity was established based on the geological engineering characteristics of a karst site. The results show that the subgrade stability is controlled by multiple factors related to the upper load, the stability of the caves, and the soil state; increasing the upper load of the track further develops the sinkhole and has a negative effect on the subgrade stability. The amplitude of vertical dynamic displacement on the subgrade surface can reach 1.31 mm under the superimposed effect of the vibration of double railways, which is approximately 50% higher than that of a single railway. Under the long-term cumulative effect of train vibrations, the sinkholes grow faster in dynamic displacement amplitude than the roadbed surface, and will lead to abrupt displacement of subgrade surface.

1. Introduction

China is one of the countries with the largest karst presence, and the karst collapse development area is 560,000 km^2. At present, the mileage of the "Eight Vertical and Eight Horizontal" main high-speed railway in the highly prone area of karst collapse has reached 1,373 km (Xiao, 2019). Owing to the continuing extension of railway lines, they are easily affected by complex geological engineering conditions and the hydrogeological environment when running through karst areas (Fan et al., 2018). Under the long-term actions of train vibration and the underground water level, the loose overburden can collapse, which negatively affects the safe running of trains (Gutiérrez et al., 2018).

Karst collapse is frequently attributed to the subduction caused by a drop in the groundwater level. The natural environment can induce karst collapse during changes in water level caused by rainfall or pumping (Buckerfield et al., 2019); however, man-made vibration will also induce the development of overburden karst collapse (Xiao et al., 2018), which leads to the generation of different shapes of sinkholes under different dynamic conditions (Czerewko et al., 2019). A sinkhole generated under the subgrade will lead to uneven settlement and deformation damage to the subgrade surface, and the instability of the subgrade slope and the instability of the subsidence of the cave will lead to subgrade collapse (Xu et al., 2017). Even stable cavities in their natural state can collapse from engineering disturbances during the construction period and railroad vibrations during the operational period (Cui et al., 2015).Whether naturally formed or man-made, a sinkhole may develop upward. When the roof plate of the sinkhole is insufficient to support the upper load, instability of the slope of the roadbed, uneven settlement of the roadbed, deformation of the roadbed and track structure, and even collapse of the subgrade may occur (Kaufmann and Romanov, 2016; Xiao et al., 2018). Due to the weight of the overburden soil and the action of train vibration, sinkhole under the subgrade is prone to deformation and collapse, which affect the stability of the subgrade, especially when the overlying soil layer of sinkhole is shallow (Wang et al., 2017).

CORRESPONDENCE Mingzhou Bai mzhbai@bjtu.edu.cn School of Civil Engineering, Beijing Jiaotong University, Beijing 100044, China; Beijing Key Laboratory of Track Engineering, Beijing Jiaotong University, Beijing 100044, China

At present, during the construction of railroad subgrades, the underlying karst caves within a certain range of the railway project are grouted or reinforced (He et al., 2016), but the impact of construction on the foundation soil is quite different from the effect of traffic vibration loading during the operational period. Karst collapse caused by blasting vibration (Kaláb et al., 2013), tunnel envelope excavation (Zhong et al., 2012), and pile driving during the construction period is mainly attributable to a water leakage-type collapse (Li et al., 2013), whereas those during the operational period transform into stable phase karst collapse under long-term action (Zhou et al., 2019). With the increase in train speeds, the nonlinear vibration effect of the train is further strengthened (Jiang and Gao, 2020), and the cumulative effect of the generated low-frequency and low-amplitude vibration promotes the development of sinkholes in the karst area and adversely affects the subsoil of the subgrade, furthering the destabilization of the railroad roadbed during the operational period (Sebastian and Steffen, 2018).

Current research on train vibration transmission mainly concentrates on the analysis of track vibration reduction, environmental noise reduction, and bridge and tunnel enclosure stability, etc., exploring the distribution of stress and strain in the roadbed structure under train loads such as different train axle weights and travel speeds (Zhao et al., 2015), studying the wheel load response of natural in-situ soil samples under cyclic loads (Cai et al., 2016), or investigating the factors that influence train vibration transmission in the region (Ma et al., 2019). According to the characteristics of z, the nonlinear model of track-roadbed coupling is established by numerical simulation considering the detailed characteristics of track structure. Furthermore, the relationship between train vibration effect and track structure is analyzed in depth from the aspects of deformation characteristics of track structure, vibration response of roadbed soil, etc. (Quinn et al., 2010; Alabbasi and Hussein, 2019). However, the vibration transmission law of high-speed trains in special strata of karst areas, as well as the long-term cumulative effect of low-frequency, low-amplitude vibration on the roadbed stability and sinkhole state have not been systematically studied.

Considering the above research deficiencies, this study establishes a vehicle–track–subgrade coupling model based on the geomorphological conditions in karst areas. The propagation characteristics of train vibration waves in subgrade containing sinkhole were analyzed, the dynamic response characteristics of roadbed sinkhole locations, and the long-term cumulative effect of train vibrations on the stability of the roadbed.

2. Methods

The ABAQUS software based on FEM was used to establish the model matching the actual structure size and carry out the train vibration loading. in this study. As a typical non-uniform material, the dynamic coupling model of vehicle-track-subgrade has nonlinear properties, and its vibration wave has obvious directivity. In roadbed, a train vibration wave can be regarded as a linear vibration source, and the propagation law is shown in Fig. 1. According to the above characteristics, the ABAQUS/Standard module was used to balance its initial static state, and the ABAQUS/Explicit module was used to analyze its dynamic load.

2.1 Vehicle–Track Coupling Model

A high-speed train is a system of spring–damper suspension devices, wheelsets, bogies, and carriages. As the main research object of this paper is the vibration load generated by the train operation, the train model was simplified into a structure composed of wheelset, carriage, and bogie according to the actual size to achieve the purpose of simulating its vibration wave generation, where each component was connected by suspension systems.

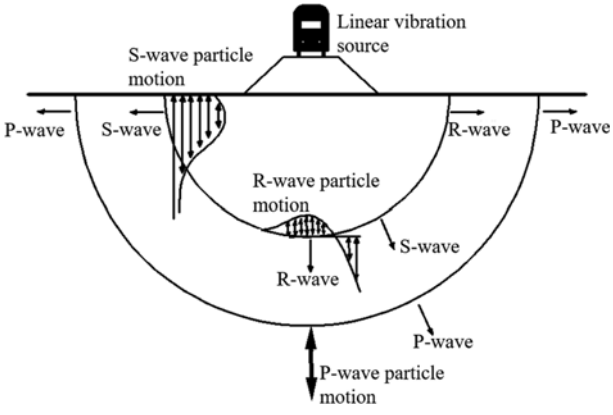

Fig. 1. Propagation Characteristics of Vibration Wave under a Linear Source

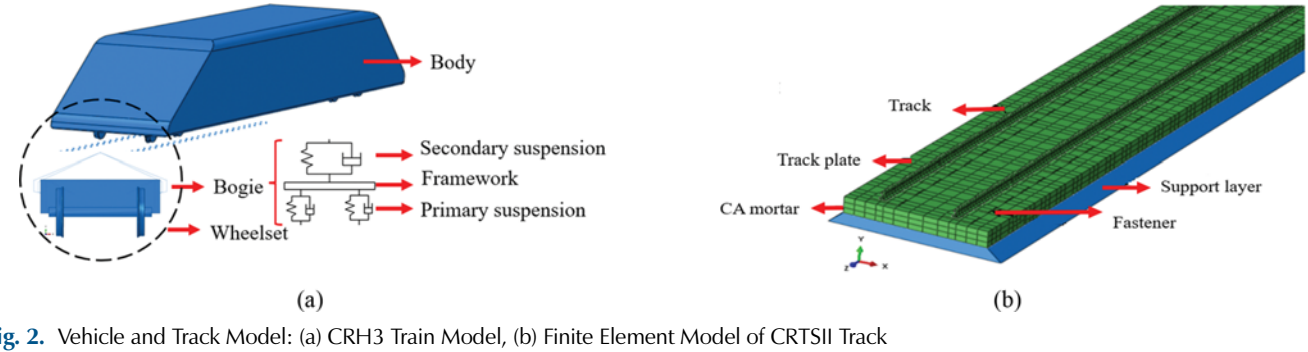

Fig. 2. Vehicle and Track Model: (a) CRH3 Train Model, (b) Finite Element Model of CRTSII Track

The CRH3 train and CRTSII ballastless track, which are common along the route of the Shanghai-Kunming high-speed railway (Guizhou section) with high incidence of karst phenomena, were used as modeling prototypes. During the simulation, rails, fasteners, track plates, cement asphalt (CA) mortar, and supporting layers were considered, where the components were connected by the Tie constraint of ABAQUS. The train–track model established is shown in Fig. 2.

The model considers the normal and tangential force between the wheel and the track due to the contact action, the former using the Hertz nonlinear elastic contact model and the latter was determined by the vertical force and friction coefficient between the wheel rails (Wang et al., 2018). The random process theory was applied to track irregularity to simulate the real wheel–rail vibration associated with deviations of track shape, geometric size, and position in space.

The track was represented as an elastic model without plastic deformation. The relevant material parameters of the vehicle–track model, Rayleigh damping coefficients α and β, and calculation parameters of the fasteners are shown in Table 1 (Xu et al., 2020).

2.2 Subgrade-Sinkhole Model

Based on the actual engineering geological profile of the study area, and according to the requirements of TB 10621-2014 High-speed Railroad Design Specification, the single and double track subgrade width was selected as 8.6 m and 13.6 m, respectively; the length of the railway line direction was 50 m, the width of the direction perpendicular to the railway line was 50 m, the height of the subgrade was 27 m, and the slope ratio of the subgrade side was modeled as 1:1.5. The sinkhole was set under the subgrade and connected through the karst network to simulate natural karst development in soluble rock, and the sinkhole was located in the center of the model, along the train forward length at 30 m. Fig. 3 shows the schematic of the final vehicle–track–subgrade coupled single and double railway models with a model size of 50 m (railway direction) by 50 m by 30 m. A continuous spring-damping element system was used at the bottom of the model to simulate the viscoelastic boundary.

Considering the plastic deformation of both the roadbed structure and the geotechnical body of the foundation at the time of analysis, the Mohr–Coulomb ideal elastic–plastic material

Table 1. Calculation Parameters for Vehicle–Track Model Structure

Structural layer	Parameters	Value	Structural layer	Parameters	Value
Track	Elastic modulus / GPa	210	CA mortar	Elastic modulus / MPa	7,000
	Poisson's ratio	0.3		Poisson's ratio	0.2
	Sectional area / cm^3	76.45		Thickness / m	0.03
	Density / $kg{\cdot}m^{-3}$	7,800		Density / $kg{\cdot}m^{-3}$	1,800
	α / s^{-1}	0.0328		α / s^{-1}	0.0983
	β / s^{-1}	0.0031		β / s^{-1}	0.0092
Track plate	Elastic modulus / GPa	35.5	Support layer	Elastic modulus / GPa	22
	Poisson's ratio	0.2		Poisson's ratio	0.2
	Length×Width×Thickness / m×m×m	100×2.55× 0.2		Span×Thickness / m×m	(2.95/3.25)×0.3
	Density / $kg{\cdot}m^{-3}$	2,500		Density / $kg{\cdot}m^{-3}$	2,500
	α/ s^{-1}	0.0983		α/ s^{-1}	0.0983
	β/ s^{-1}	0.0092		β/ s^{-1}	0.0092
Fastener	Vertical stiffness / $N{\cdot}m^{-1}$	4.5×10^7	Fastener	Vertical damping / $N{\cdot}s{\cdot}m^{-1}$	6.0×10^4
	Transverse stiffness / $N{\cdot}m^{-1}$	3.0×10^2		Transverse damping / $N{\cdot}s{\cdot}m^{-1}$	3.625×10^4

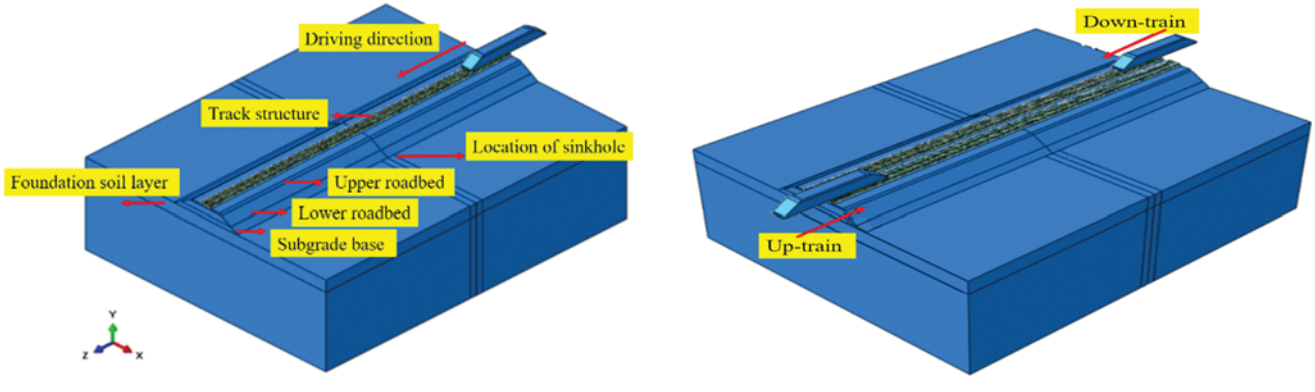

Fig. 3. Vehicle-Track Subgrade Coupling Model for Single and Double Railways: (a) Single Railway (b) Double Railway

Table 2. Material Parameters of Subgrade and the Bedrock

Type	Elastic module / MPa	Poisson's ratio	Density / g·cm^{-3}	Cohesive force / KPa	Inner friction angle / °
Top of the subgrade bed	220	0.25	2.1	35	43
Bottom of the roadbed	130	0.3	1.9	13	28
Ground	50	0.2	1.8	30	25
Limestone	190	0.25	2.6	20	44.3
First layer of soil (1 m)	14.5	0.25	1.6	31	25
Second layer of soil (2 m)	15.7	0.25	1.8	32	24
Third layer of soil (3 m)	17.3	0.25	1.9	34	26

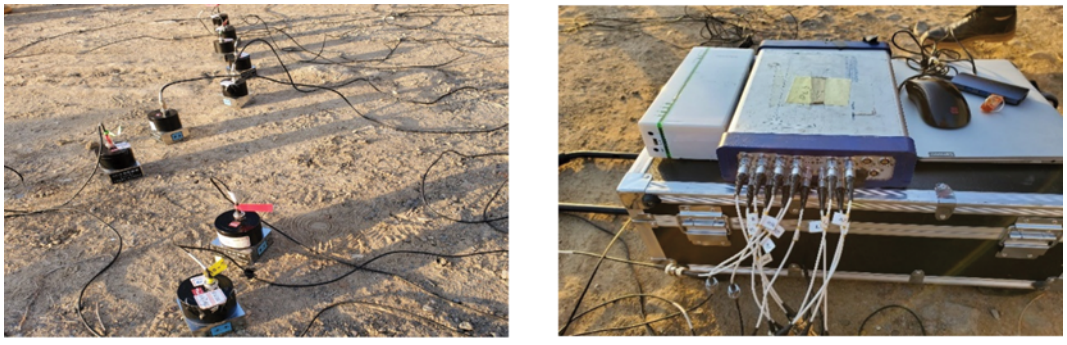

(a) (b)

Fig. 4. Equipment Used for Field Monitoring: (a) Model 291-2 Vibration Picker, (b) Data Acquisition Instrument

ontological model was used for the roadbed and geotechnical body of the foundation.

Indoor geotechnical tests were carried out on the unmodified soil of different soil layers along the railroad line in the karst region, and the mechanical parameters of the subgrade soil were determined. X-ray diffraction analysis showed that the soil was mainly cohesive soil composed of silicate and clay minerals, and the material parameters of subgrade and the bedrock are summarized in Table 2.

2.3 Model Validation

Considering the special hydrogeological features of karst areas, the experimental conditions in this study assumed the existence of groundwater with initial pore water pressure and in situ stress equilibrium. Taking an elliptical sinkhole with a span of 2.5 m and a height of 1.5 m as an example, the initial displacement magnitude of the entire site in both the vertical and horizontal direction was 10^{-6} m.

The train vibration monitoring area is located along the Shanghai-Kunming high-speed railway DK820+955 to DK821+200 in Zhenning County. The region along the railroad line mainly consists of dolomite and carbonate, strong tectonic movement, complex geological structure, and mostly covered karst, and the main damage type is karst collapse.

The vibration monitoring equipment is the 291-2 vibration picker developed by China Earthquake Administration, as shown in Fig. 4. The acceleration resolution of the equipment is 1×10^{-5} m/s^2, and the maximum vibration acceleration that can be monitored is 40 m/s^2. The data acquisition instrument developed by Beijing Oriental Institute of Vibration and Noise Technology was used with DASP software.

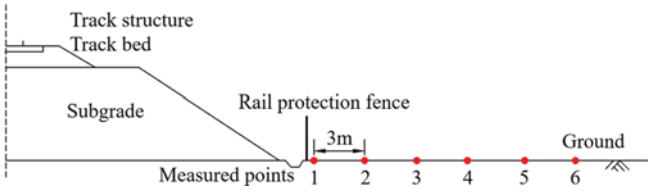

Fig. 5. Field Monitoring Points Layout

Figure 5 is the schematic diagram of the vibration wave monitoring points layout, and the monitoring section is perpendicular to the direction of the railway line. There are 6 monitoring points in total, the horizontal distance between adjacent points is 3 m, and the foot of the embankment is the first point. The height of the subgrade at the measurement section is 3 m.

Figure 6 shows a comparison of the vibration wave–time course curves obtained from the numerical simulation at points 1 and 4 with the vibration wave–time course curves obtained from on-site monitoring when an actual train passed at a speed of 229 km/h, and the monitoring train was a CRH3 high-speed train consistent with the numerical model.

The vibration acceleration amplitude of numerical simulation and field monitoring at the point 1 were 0.168 and 0.153 m/s^2, respectively, with an error of 9%. At the point 4, the values were 0.075 and 0.054 m/s^2, respectively, with an error of 38.89%. Combined with the actual terrain conditions, the errors were

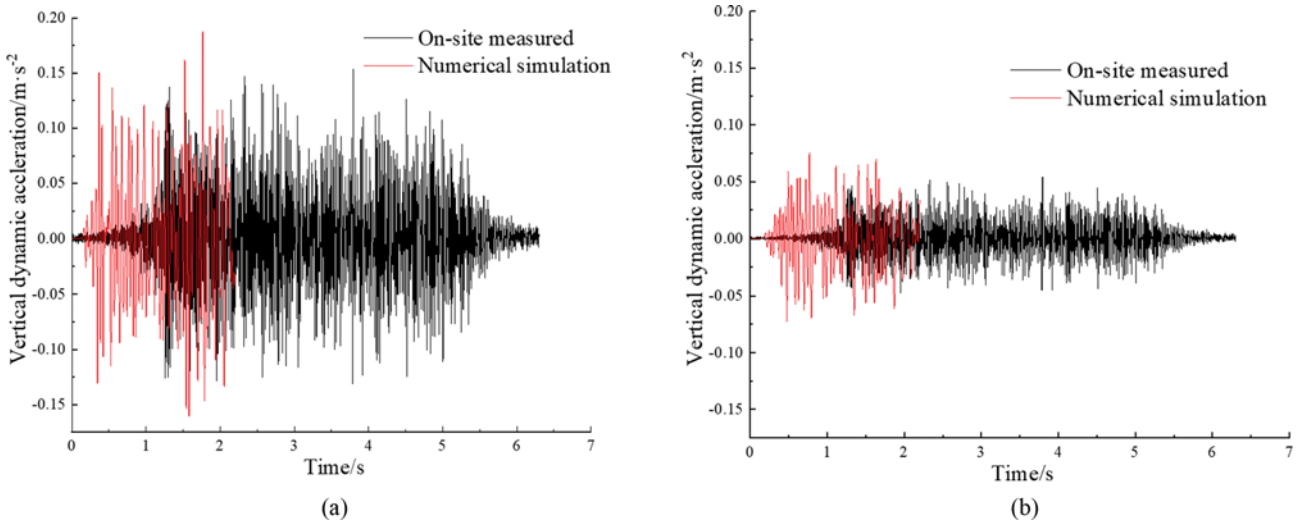

Fig. 6. Time Curves of Vibration Waves: (a) Measured Point 1, (b) Point 4

divided into two reasons. First, the field ground flora and rural soil roads have an attenuation effect on the propagation of vibration wave, so the field monitoring of vibration wave amplitude was less than the results of numerical simulation; Second, the numerical model takes the soil damping as a fixed value, while there are differences in the damping values of the soil at different locations in the field, which also leads to the increasing error of numerical simulation and field monitoring as the propagation distance of vibration wave increases.

The above analysis indicates that the farther the measuring point is from the roadbed, the greater the error of the numerical model is. However, as the vibration wave rapidly attenuates with the propagation distance, the influence of train vibration is mainly concentrated near the roadbed, and the influence on the distant soil is weak. Therefore, the model parameters and boundary conditions presented in this paper are reasonable and can effectively analyze the dynamic response near the roadbed.

3. Results

The dynamic load analysis was based on the elastic wave characteristics caused by vehicle wheel–rail vibration. The axle weight of the train was set to 16 t; the travel speed was 250 km/h; the height of the subgrade was 4 m; the overburden of the sinkhole was 2 m, and the span was 1 m.

3.1 Parameters of Train Vibration Wave

3.1.1 Vertical Vibration Acceleration

Vertical vibration acceleration (VVA) can reflect the strength of train vibration load, and also reflects the comprehensive effect of static and dynamic force of train on the subgrade. It is an important parameter to study the relationship between train vibration and subgrade. Fig. 7 shows the time curve of VVA in

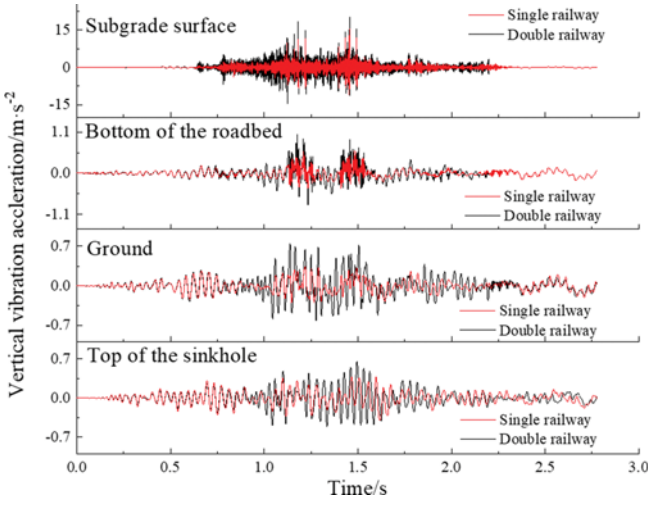

Fig. 7. Time Curve of VVA at Different Structural Layers

the whole running process of railway. It can be seen that VVA along the depth direction under the double railway condition was significantly greater than that for the single railway, the dynamic characteristics of train vibration are more obvious when the double railway is in motion, and the vibration impact frequency of the soil is more intensive and the vibration intensity is greater.

Figure 8 shows the amplitude of VVA when the train runs directly above the central sinkhole in the subgrade. Compared with the subgrade surface, VVA attenuates about 47.36%, 21.55% and 65.78% at the bottom of the roadbed, ground surface, and top of the sinkhole under the single railway, respectively, and attenuated to approximately 44.54%, 65.06% and 69.29% under the double railway driving condition. It shows that VVA becomes increasingly smaller with increasing depth, and the attenuation was mainly in the roadbed layer; Due to the reflection of vibration waves by bedrock, the rebound of VVA occurs at the location near the sinkhole.

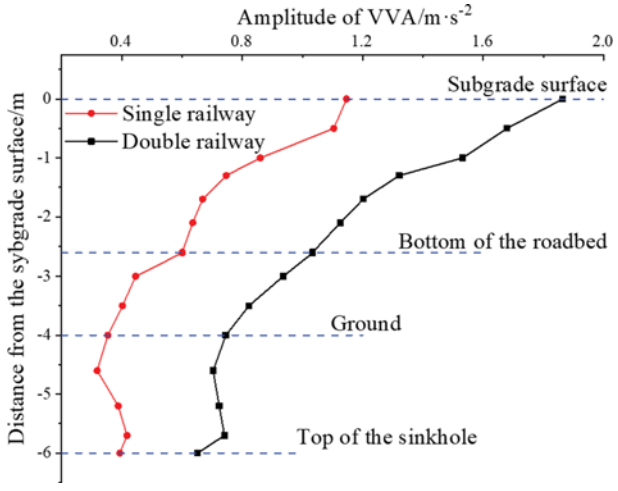

Fig. 8. Amplitude of VVA at Different Structural Layers

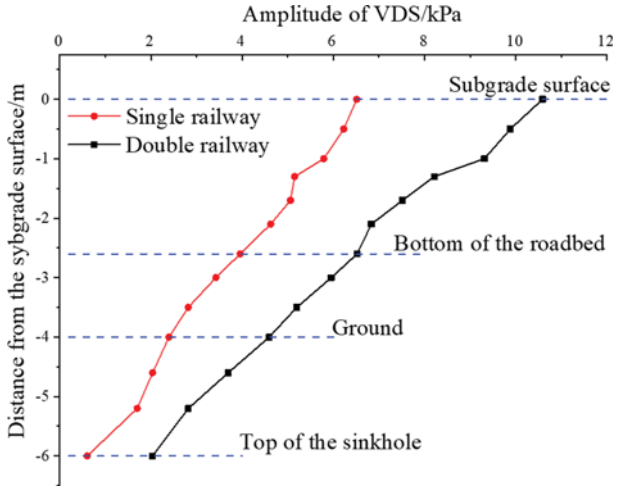

Fig. 10. Amplitude of VDS at Different Structural Layers

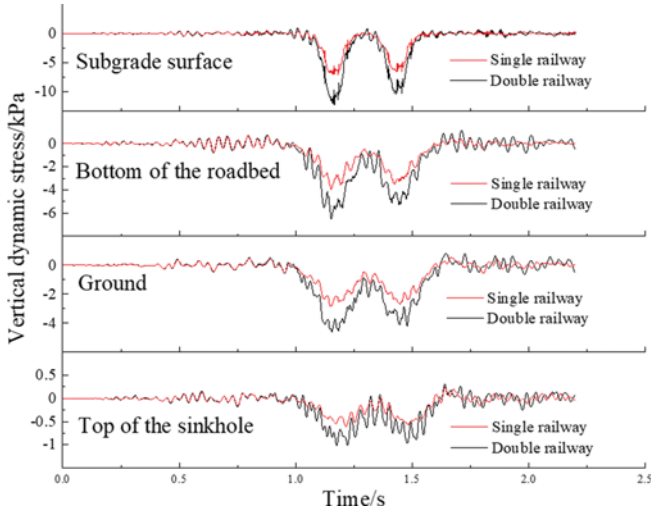

Fig. 9. Time Curve of VDS at Different Structural Layers

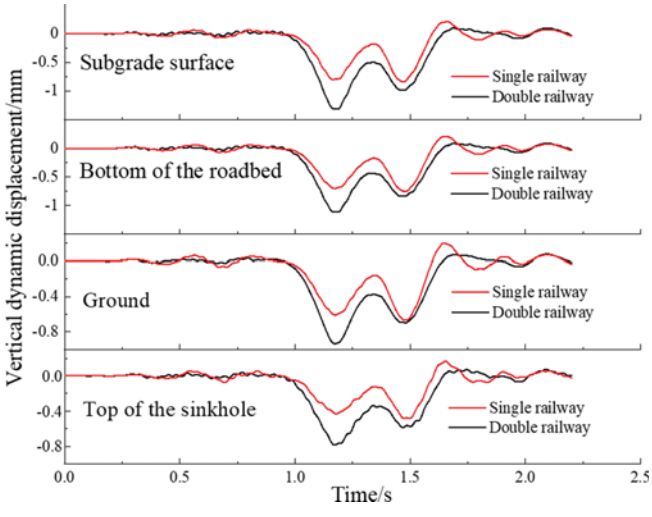

Fig. 11. Time Curve of VDD of Different Structural Layers

3.1.2 Vertical Dynamic Stress

Vertical dynamic stress (VDS) can reflect the deformation trend and position of subgrade and sinkhole under train vibration, and it is also an index to reflect its stress characteristics. Fig. 9 shows the time curve of VDS in the whole running process of railway. It shows that the maximum VDS of the subgrade surface was 12.37 kPa when the double railway running, which was 72.04% higher than that for the single railway; The maximum VDS at the bottom of the roadbed, ground surface, and top of the sinkhole for the double railway was 6.52 kPa, 4.60 kPa, and 2.03 kPa, respectively, which was 64.65%, 63.12% and 232.79% higher than those of the single railway.

Figure 10 shows the amplitude of VDS when the train runs directly above the central sinkhole in the subgrade, it can be seen that VDS attenuates almost linearly along the depth direction in both driving conditions. Compared with the subgrade surface, VDS attenuated approximately 39.22%, 63.19%, and 90.71% at the bottom of the roadbed, ground surface, and top of the sinkhole, under the single railway, respectively, and attenuated approximately 38.39%, 56.6%, and 80.78% under the double railway driving condition. The attenuation rates at different depths under the two railway conditions were basically the same, and VDS at each depth under the double railway condition was larger than that under the single condition.

3.1.3 Vertical Dynamic Displacement

Vertical dynamic displacement (VDD) is the most direct index to reflect the deformation characteristics of each structure. Fig. 11 shows the time curve of VDD in the whole running process of railway. It shows that the maximum VDD of the subgrade surface was 1.31 mm a when the double railway running, which was 56.87% higher than that for the single railway, and the displacement caused by only one vibration of double railways reached nearly 10% of the maximum allowable value of 15 mm in Code for Railway Subgrade Design (TB 10001-2016). The maximum VDD at the bottom of the roadbed, ground surface, and top of the sinkhole for the double railway was 1.05 mm, 0.93 mm, and 0.68 mm, respectively, which was 39.39%, 39.82%, and 41.49%

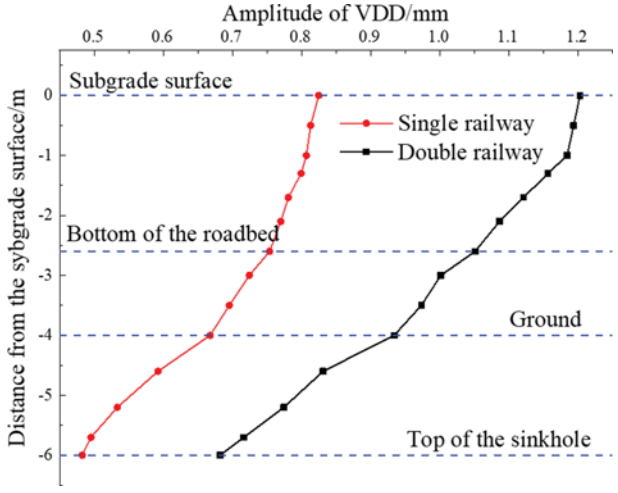

Fig. 12. Amplitude of VDD at Different Structural Layerss

higher than those of the single railway.

Figure 12 shows the amplitude of VDD when the train runs directly above the central sinkhole in the subgrade, which demonstrates a nonlinear variation along the depth direction in both railway conditions. Compared with the subgrade surface, VDD attenuated approximately 8.62%, 19.05% and 41.5% at the bottom of the roadbed, ground surface, and top of the sinkhole, under the single railway, respectively, and attenuated approximately 12.63%, 22.36%, and 43.31% under the double railway driving condition. That is, VDD attenuation area under traffic conditions was mainly concentrated below the ground surface layer.

3.2 Influencing Factors

In the development of sinkholes, the overburden thickness decreases continuously, and the relative positions of sinkholes and subgrade are complex and vary under actual conditions. In this section, the sinkhole overburden thickness and the horizontal distance between sinkholes and the subgrade are changed to analyze the dynamic response characteristics under different conditions.

3.2.1 Overburden Thickness

The primary characteristic of sinkhole development in the vertical direction is the reduction in the overburden thickness. Five conditions of the overburden thickness of sinkholes were modeled: 1.0 m, 1.5 m, 2.0 m, 2.5 m, and 3.0 m. The sinkholes were all placed directly below the subgrade.

Figure 13 shows the time curve of VDD on the subgrade surface under different sinkhole overburden thicknesses. When the overburden thickness of the sinkholes increased from 1 m to 1.5 m, 2 m, 2.5 m and 3 m, the amplitude of VDD at the subgrade surface of the single railway decreased from 0.96 mm to 0.88 mm, 0.82 mm, 0.75 mm, 0.69 mm and 0.59 mm, whereas that of the double railway decreased from 1.52 mm to 1.39 mm, 1.31 mm, 1.21 mm and 1.14 mm. As the overburden thickness increase, the amplitude of VDD on each structure almost maintained a linear decrease, indicating that the attenuation rate of the vertical dynamic displacement was related to the transmission

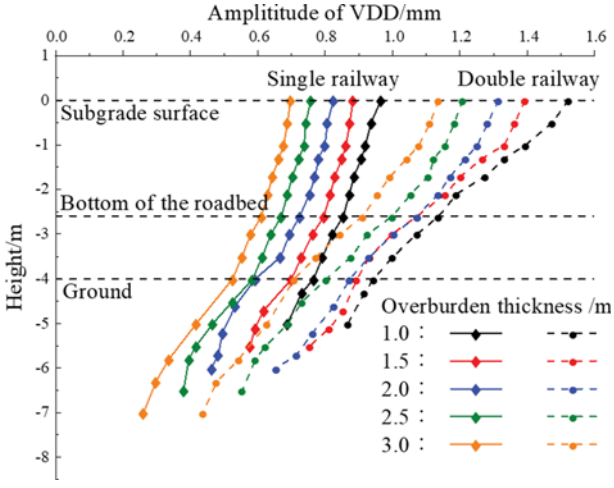

Fig. 14. Amplitude of VDD of Subgrade Centerline

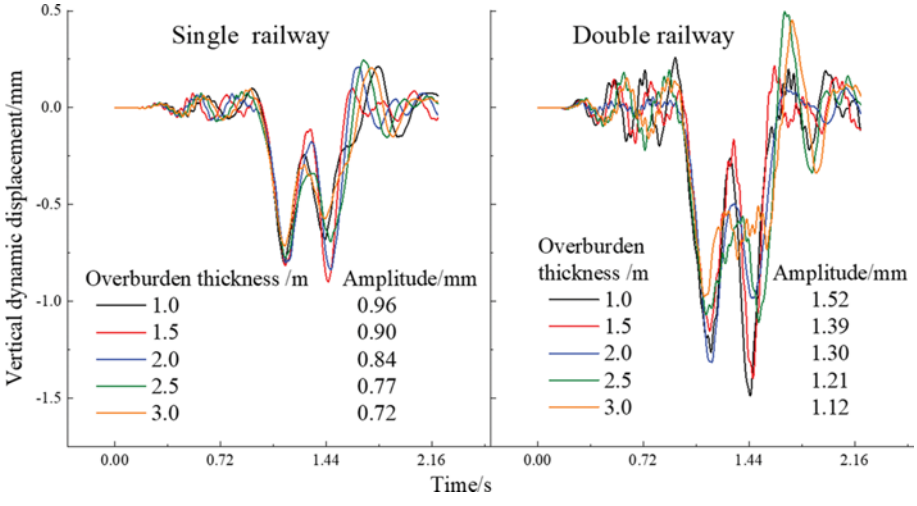

Fig. 13. Time Curve of VDD on Subgrade Surface

distance.

Figures 14 and 15 shows amplitude of VDD and the attenuation coefficient for the double railway with different depths. When the overburden thickness was 1.0 m, 1.5 m, 2.0 m, 2.5 m, and 3.0 m, the amplitude of VDD from the subgrade surface to the top of the sinkhole attenuated by 26.87%, 34.58%, 41.50%, 45.97%, and 62.54%, respectively. The sinkhole with the thin overburden will be more obviously affected by the train vibration, and larger VDD of subgrade surface will produced.

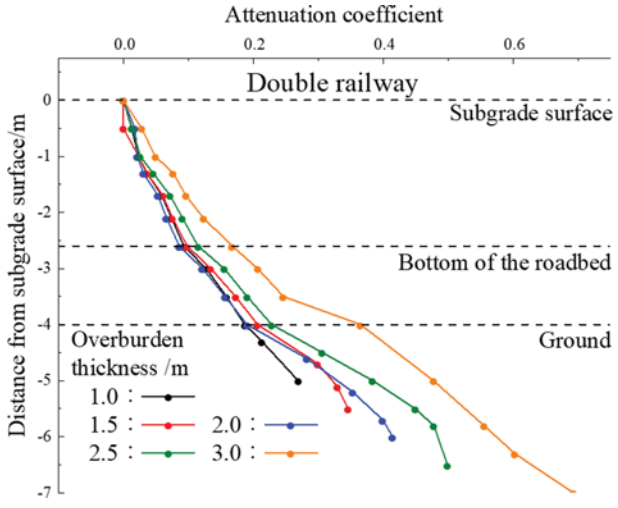

Fig. 15. Attenuation Coefficient of the Double Railway

3.2.2 Horizontal Distance between the Sinkhole and Subgrade Centerline

The horizontal distance between the top of the sinkhole and the centerline of the subgrade was modeled as 0 m (from the centerline of the subgrade), 3 m, 6 m, 10 m, and 15 m, and the modeled overburden thickness was 2 m.

Figure 16 shows the time curve of VDD on subgrade surface under different horizontal distances. When the distance increased from 0 m to 3 m 6 m 10 m and 15 m, the amplitude of VDD on the subgrade surface decreased from 1.31 mm to 1.01 mm 0.82 mm 0.67 mm and 0.59 mm under the double railway, a reduction of 22.9%, 37.4%, 48.85% and 54.96%, respectively, and the corresponding decrease rate of single railway is 30.95%, 39.28%,

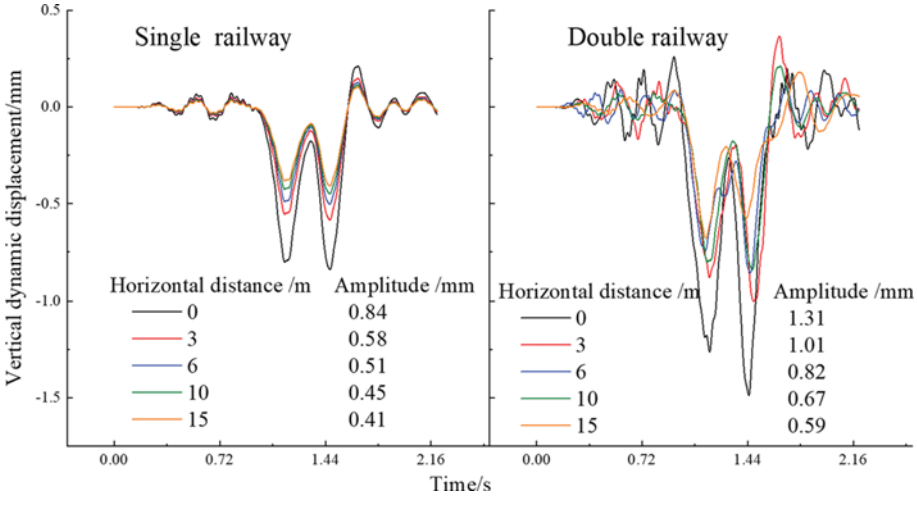

Fig. 16. Time Curve of VDD on Subgrade Surface

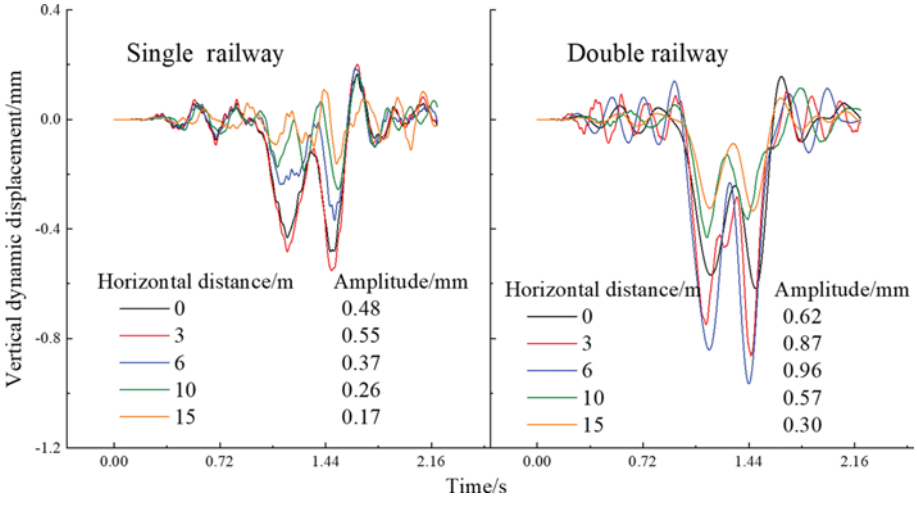

Fig. 17. Time Curve of Vertical Dynamic Displacement at the Top of the Sinkhole

46.42% and 51.19 %. It can be seen that as the distance to the sinkhole increased, the amplitude of VDD on the surface decreased nonlinearly.

Figure 17 shows the time curve of VDD on the top of the sinkhole under different horizontal distances. Different from the effect of changing the overburden thickness, the amplitude of VDD on the top of the sinkhole first increased and then decreased as the horizontal distance between the subgrade and the sinkhole increased.

This is due to the fact that, when the horizontal distance to the sinkhole increases, the vibration will first pass through the support layer of the track structure, where a large VDS will be concentrated. These results indicate that the closer the sinkhole is to the supporting layer of the track structure, the larger the VDD at the top of the sinkhole will be, which affects the stability of the sinkhole and thus the stability of the subgrade.

3.3 Different Number of Train Vibrations

The vibration waveform in Section 2.3 was repeatedly loaded on the track superstructure to simulate the long-term train vibrations and analyze the cumulative effect, and each loading represents the complete passes process of single or double train.

Figure 18 shows the amplitude of VDD of each structural layer under different numbers of train vibrations. With an increase in the number of train vibrations, the amplitude of VDD at each layer of the subgrade structure and the top of the sinkhole increased, and the amplitude of VDD at each structure for double railway was greater than that for single railway. The amplitude of VDD on the subgrade surface increased from 1.68 mm to 1.73 mm, 1.78 mm, 1.84 mm, 1.91 mm, and 1.99 mm when the number of cyclic loads increased from 1 to 10, 100, 1000, 5000, and 10,000 times, respectively, with relative increases of 2.97%, 5.95%, 9.52%, 13.69%, and 18.45%. The amplitude of VDD and the number of loadings maintained almost logarithmic growth, and VDD on subgrade surface under long-term vibration tended to be stable.

Figure 19 shows the displacement contour when the single train vibration load reaches 100,000 times (the deformation in Fig. 19(b) was magnified by 30 times). It can be seen that under the long-term vibration load, the displacement range of the subgrade surface is still far from the model boundary, indicating that the model size is reasonable. It can be seen that the displacement

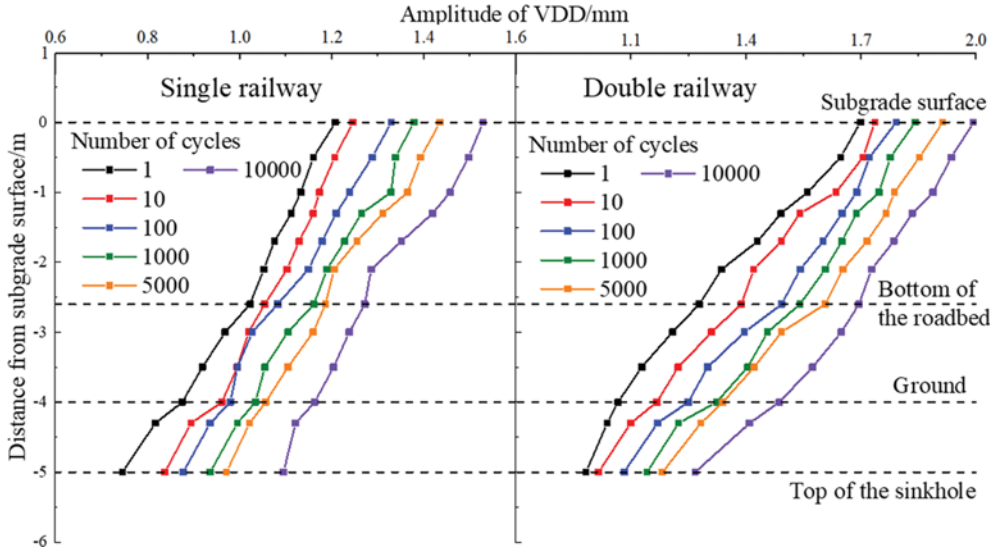

Fig. 18. Amplitude of Vertical Dynamic Displacement under the Cyclic Load

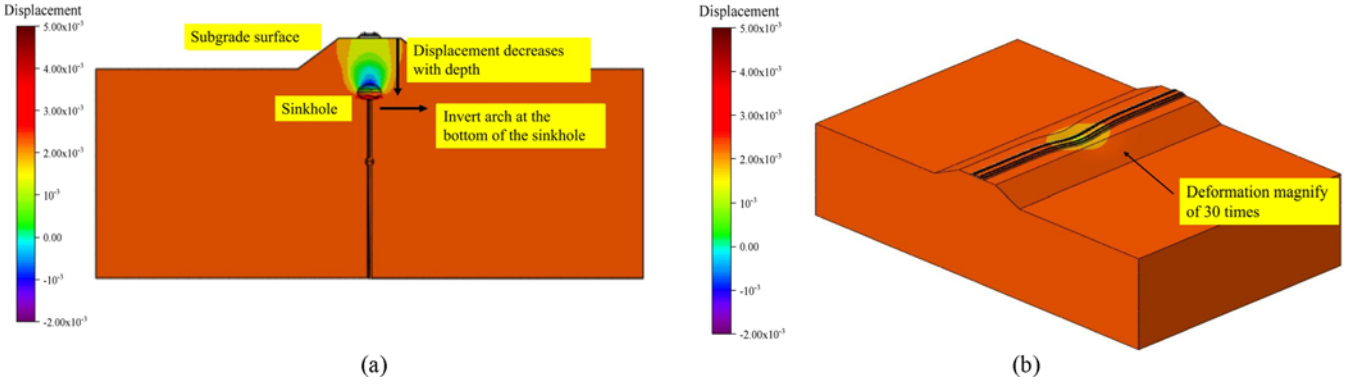

Fig. 19. Displacement Contour: (a) Center Section of Model, (b) Overall Model

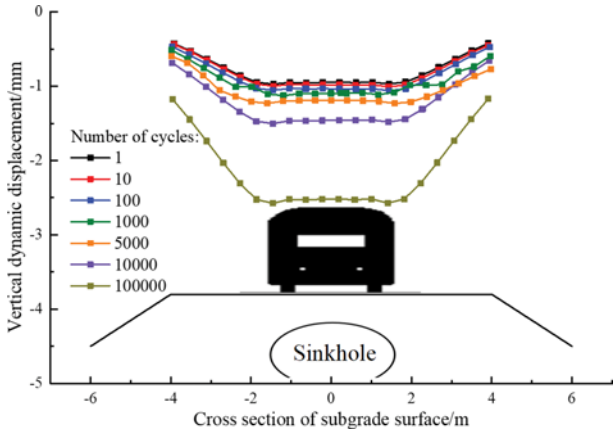

Fig. 20. Amplitude of VDD on Cross-Sectional Subgrade Surface

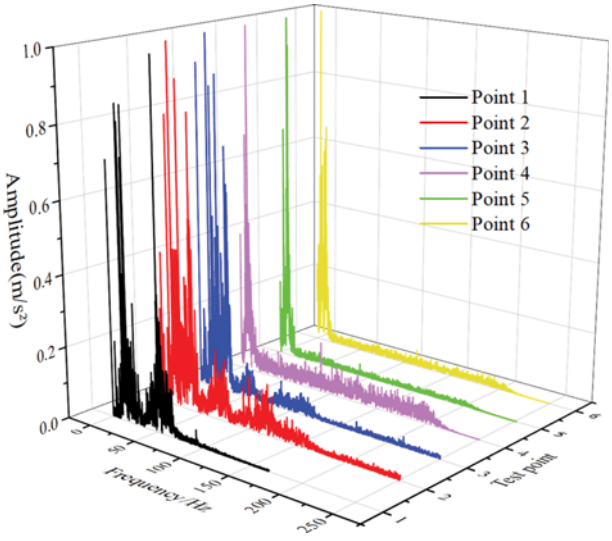

Fig. 21. Spectrum of VVA at Different Horizontal Points

from the subgrade downward is decreasing continuously, however, the displacement at the bottom of the sinkhole is much larger than that of other positions, which indicates that the sinkhole produces large deformation under long-term vibration, and its scale keeps expanding, and finally causes the instability failure of the subgrade. It's mean that the stability of subgrade is controlled by the stability of sinkhole under the long-term train vibration load.

Figure 20 shows the amplitude of VDD on cross-sectional subgrade surface under different numbers of train cycles, it can be seen that the uneven settlement of the subgrade surface was produced. This is due to the existence of sinkhole, the subsidence rate of the soil above the sinkhole is significantly higher than other locations, resulting in the settlement depth of the subgrade surface above the sinkhole is obviously greater. The vertical displacement of the subgrade surface is symmetrically distributed along the center line of the subgrade, the settlement directly below the track is slightly larger than that on both sides, and the overall settlement of the subgrade surface is in a shape of "basin". When the number of vibration cycles reaches 100,000, the amplitude of VDD on subgrade surface reached 2.68 mm, which is significantly increased compared with that of 10,000 cycles actions.

4. Discussion

4.1 Kinetic Characteristics of Train Vibration

Figure 21 shows the spectrum curve obtained after Fourier transform of the time history signals of VVA at six measuring points outward from subgrade slope foot; it can be seen that there are more high-frequency components of vibration near the subgrade, and the frequency distribution of vibration is more extensive. The dominant frequency of vibration is reduced from 20 – 60 Hz at the subgrade slope foot to 0 – 10 Hz at the farthest distance from the roadbed, and almost all vibration of 20 – 60 Hz is dissipated in the transmission path. This indicates that as the vibration wave transmission distance increases, high-frequency vibration decays faster, resulting in progressively lower peak values of the spectrum curve, and the vibration intensity gradually decreases.

The above phenomenon can be attributed to the existence of soil damping, when the vibration wave transmission distance is the same, the high-frequency vibration wave causes more vibration of the soil particles, and more energy is consumed by the friction between soil particles; thus, the inhibition effect of soil on high-frequency vibration is more obvious. This is also why the train vibration will not significantly promote the development of the sinkhole with a long distance and further affect the stability of the subgrade structure.

4.2 Difference of Vibration between Single and Double Railways

The vibration response under the condition of the double railway is larger than that of a single railway, in which the vibration acceleration generated near the ground is doubled, and the dynamic stress at the top of the sinkhole reaches twice as much as that of the single railway. This means that with increasing train vibration load, the impact on the sinkhole will become increasingly intense, and the development of the sinkhole will increase non-linearly.

Figure 22 shows the contour of the VDD of single and double railways as they travel to the subgrade directly above the sinkhole. As can be seen, the trends in VDD of single and double railways were generally the same, but the double railway showed greater displacement at each structural layer because of the direct increase in the upper load.

It is found that with the increase of train vibration wave frequency (the train speed is increased), the VDD of subgrade surface increases non-linearly, while the train axle load is increased and the train speed remains unchanged, VDD of subgrade surface basically maintains a linear growth relationship (Li et al., 2021). This shows that the variation of vibration wave frequency is the main reason for the non-linear growth of VDD. Compared

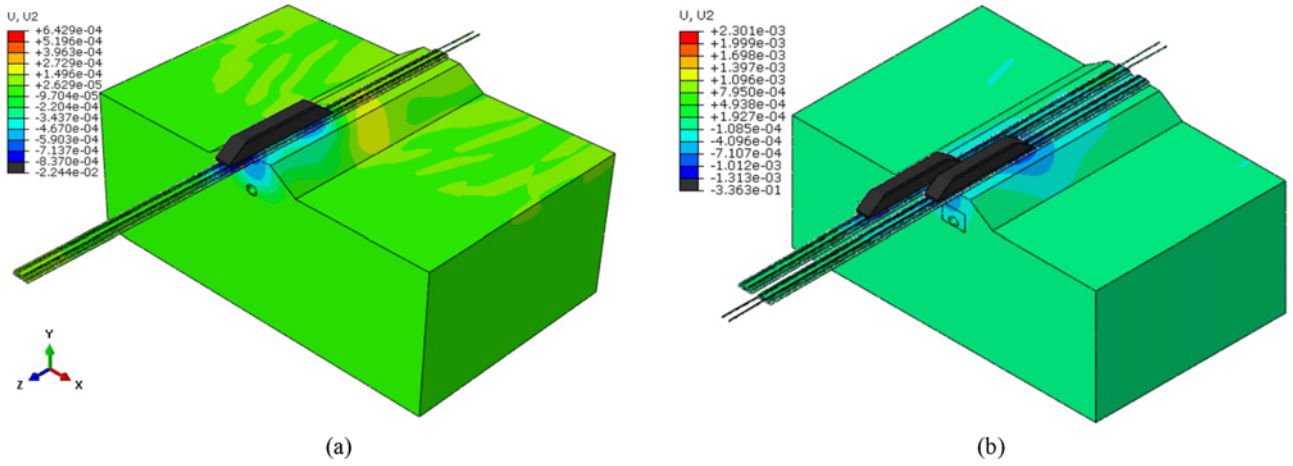

Fig. 22. Contour of VDD for the: (a) Single Railway, (b) Double Railway

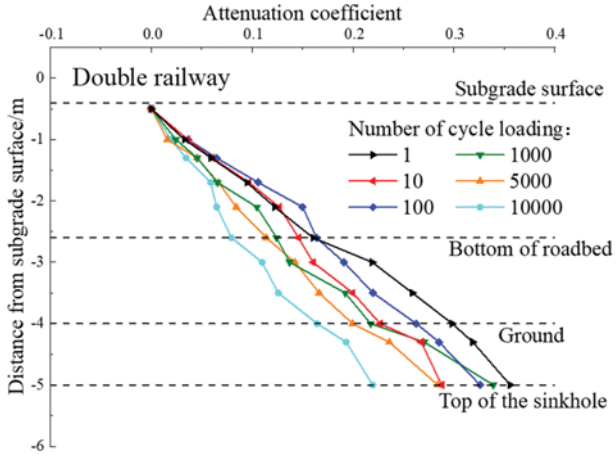

Fig. 23. Attenuation Coefficient of the Amplitude of VDD under Different Number of Cycle Loadings

with that of the single railway, the increase in the axle load of double railways also intensifies the vibration effect, and the subgrade and sinkhole will be more quickly subjected to vibration impact.

4.3 Long-Term Cumulative Effect of Train Vibrations

Figure 23 shows the attenuation coefficient of the amplitude of VDD under different numbers of cyclic. As the number of cycle loadings increases from 1 to 10000, the amplitude of VDD from the subgrade surface to the top of the sinkhole increased, and the decay rate of the VDD became slower. That is, the deformation of the subgrade surface caused by train vibration shows a large initial displacement and slow development, while the underground sinkhole shows a small initial displacement and fast development. Under the cyclic load, the amplitude of VDD and cyclic numbers almost maintain logarithmic growth, and the amplitude of VDD on the subgrade surface tends to be stable under long-term cyclic vibration.

In fact, the existence of sinkholes will loosen the surrounding soil and reduce the density of subgrade soil around the sinkhole. Meanwhile, the expansion of sinkholes will also make soil particles squeeze each other and increase the density of soil in some areas. The opposite trend will prevent the deformation of the sinkhole, so that the sinkhole will not grow infinitely rapidly with the increase in the number of train vibrations, and its expansion trend will gradually slow down (Wang, 2014).

4.4 Critical Instability Condition of Roadbed

The strength reduction method is often used in the stability analysis of slopes, mining areas and karst collapse, where the cohesion c and internal friction angle φ of the soil are simultaneously divided by the strength reduction factor F to obtain a new set of c_m and φ_m, as shown in Eq. (1). When F_s is greater than 1, it means that the roadbed under this calculation condition is in a stable state.

This process is realized by modifying the model input file of Edit Keywords in ABAQUS, and F is gradually increased to achieve the reduction of soil strength in the calculation. When the displacement mutation causes the calculation to diverge, it means that the subgrade soil reaches the critical instability state, at this time F is the safety strength reduction factor F_s:

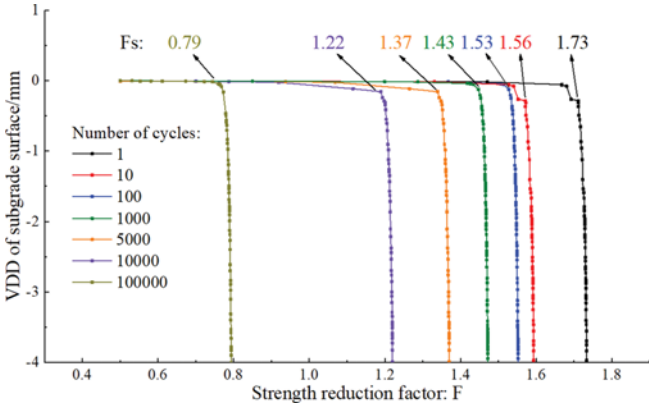

Fig. 24. The Relationship between Strength Reduction Factor and Numbers of Cycles

$$\frac{c}{c_m} = \frac{\tan\varphi}{\tan\varphi_m} = F(F_s)\,. \quad (1)$$

In Eq. (1), c and φ are the initial parameter of soil, c_m and φ_m are the parameters of soil under the safety strength reduction factor.

Figure 24 shows relationship between the amplitude of VDD on subgrade surface and F under the action of different numbers of cycle times, and the values of F_s were marked in the figure. When the number of cycles is 1, 10, 100, 1,000, 5,000 and 10,000, the F_s is 1.73, 1.56, 1.53, 1.43, 1.37 and 1.22, respectively, it can be seen that the roadbed is in stable state under above number of cycles, and F_s decreases with the increase of cycle times.

When the number of cycles reaches 100,000 F_s is 0.79. Through the analysis of soil strength, it can be seen that the roadbed is difficult to maintain a stable state at this time, the displacement of subgrade surface will produce sudden changes, indicating that it has reached the critical instability state. This also corresponds to the above Section 3.3 when the number of cycles reaches 100,000, the subgrade surface has an obvious deformation.

5. Conclusions

In this study, a coupling model of vehicle–track–subgrade (including underlying sinkhole) was established based on the geological engineering characteristics of a karst site. The transmission of vibration loads in karst areas and the influence of single and double railway dynamic loads on the stability of subroad soil were analyzed. The main conclusions were as follows:

1. The train vibration increased the vertical deformation and vibration acceleration experienced at the top of the sinkhole, and the negative effects of the development of the sinkhole and train vibration on the stability of the subgrade were mutually reinforcing. The smaller the overburden thickness was, the more significant the dynamic response became and the larger the dynamic displacement amplitude was, which further aggravated the dynamic displacement on the subgrade surface.
2. The train vibration was mainly attenuated in the roadbed, with the main attenuation area of the dynamic displacement in the foundation. The vertical deformation, vibration acceleration, and dynamic stress caused by the double railway were all larger than those of the single train, and the dynamic stress at the top of the sinkhole could reach twice that of a single train.
3. When the modeled horizontal distance from the centerline of the subgrade to the sinkhole was arranged from small to large, the vertical dynamic displacement amplitude showed a trend of first increasing and then decreasing. When the sinkhole was located directly under the track supporting layer, it bore a large dynamic stress, and this caused a large dynamic displacement of the subgrade surface.
4. The deformation of the subgrade surface was logarithmically related to the cycle number of long-term train vibrations, and the decay rate of the vertical dynamic displacement amplitude from the subgrade surface to the top of the sinkhole became slower as the number of cycles increased. The growth rate of the dynamic displacement amplitude of the sinkhole was greater than that at the subgrade surface.
5. The settlement speed of soil above the sinkhole is greater than other locations, and the settlement is in a shape of "basin"; With the increase of train vibration times, the bearing capacity of the soil structure gradually decreases, and resulted in abrupt changes in the displacement of subgrade surface.

Acknowledgments

This work is supported by the Fundamental Research Funds for the Central Universities of China (no. 2020JBZ111). We would like to express our gratitude to the editors and reviewers for their constructive and helpful review comments.

ORCID

Mingzhou Bai https://orcid.org/0000-0003-4135-0990

References

Alabbasi Y, Hussein M (2019) Geomechanical modelling of railroad ballast: A review. *Archives of Computational Methods in Engineering* 28(3):815-839, DOI: 10.1007/s11831-019-09390-4

Buckerfield S, Quilliam R, Waldron S, Naylor L, Li SL, Oliver D (2019) Rainfall-driven *E. coli* transfer to the stream-conduit network observed through increasing spatial scales in mixed land-use paddy farming karst terrain. *Water Research X* 100038, DOI: 10.1016/j.wroa.2019.100038

Cai YQ, Guo L, Jardine R, Yang Z, Wang J (2016) Stress–strain response of soft clay to traffic loading. *Géotechnique* 67, DOI: 10.1680/jgeot.15.P.224

Cui QL, Wu HN, Shen SL, Xu Y, Ye GL (2015) Chinese karst geology and measures to prevent geohazards during shield tunnelling in karst region with caves. *Natural Hazards* 77, DOI: 10.1007/s11069-014-1585-6

Czerewko MA, Bastekin A, Tunnicliffe J, O'Rourke R (2019) Wind turbine construction in and around carsington pasture in derbyshire; overcoming the challenges posed by difficult ground conditions. *Quarterly Journal of Engineering Geology & Hydrogeology* 52(4): 459-480, DOI: 10.1144/qjegh2018-198

Fan H, Zhang Y, He S, Wang K, Wang X, Wang H (2018) Hazards and treatment of karst tunneling in Qinling-Daba mountainous area: Overview and lessons learnt from Yichang–Wanzhou railway system. *Environmental Earth Sciences* 77(19):679, DOI: 10.1007/s12665-018-7860-1

Gutiérrez F, Ca MZ, Linares R, Roqué CR, Rbonel DC, Guerrero J, McCalpin JP, Comas X, Cooper AH (2018) Identifying the boundaries of sinkholes and subsidence areas via trenching and establishing setback distances. *Engineering Geology* 233:255-268, DOI: 10.1016/j.enggeo.2017.12.015

He W, Li K, Wang F (2016) Large-scale experimental study of multi-

layered reinforcement to prevent underneath sinkhole in karst terrain and the design method. *Chinese Journal of Rock Mechanics and Engineering* 35:980-988, DOI: 10.13722/j.cnki.jrme.2015.1018 (in Chinese)

Jiang H, Gao L (2020) Study of the vibration-energy properties of the CRTS-III track based on the power flow method. *Symmetry* 12(1):69, DOI: 10.3390/sym12010069

Kaláb Z, Pandula B, Stolarik M, Kondela J (2013) Examples of law of seismic wave attenuation. *Metalurgjia* 52(3):387-390

Kaufmann G, Romanov D (2016) Structure and evolution of collapse sinkholes: Combined interpretation from physico-chemical modelling and geophysical field work. *Journal of Hydrology* 540:688-698, DOI: 10.1016/j.jhydrol.2016.06.050

Li X, Bai MZ, Wei ZJ, Li PX, Shi H, Zhang Y (2021) Dynamic response and stability analysis of high-speed railway subgrade in Karst areas. *IEEE Access* 9:129188-129206, DOI: 10.1109/access.2021.3113706

Li ZG, Xiao SD, Pan YH, Lu SW (2013) The hazard assessment of karst surface collapse risk zoning based on BP neural network in Wuhan city. *Applied Mechanics & Materials* 405-408:2376-2379, DOI: 10.4028/www.scientific.net/AMM.405-408.2376

Ma J, Dong L, Zhao G, Li X (2019) Ground motions induced by mining seismic events with different focal mechanisms. *International Journal of Rock Mechanics & Mining Sciences* 116:99-110, DOI: 10.1016/j.ijrmms.2019.03.009

Quinn AD, Hayward M, Baker CJ, Schmid F, Priest JA, Powrie W (2010) A full-scale experimental and modelling study of ballast flight under high-speed trains. *Proceedings of the Institution of Mechanical Engineers* 224(F2):61-74, DOI: 10.1243/09544097JRRT294

Sebastian S, Steffen M (2018) Design of railway bridges for dynamic loads due to high-speed traffic. *Engineering Structures* 174:396-406, DOI: 10.1016/j.engstruct.2018.07.030

TB10001-2016 (2016) Code for design of earthworks and track bed for railway. TB 10001-2016, National Railway Administration of the People's Republic of China, Beijing, China

TB10621-2014 (2014) Code for design of high speed railway. TB10621-2014, National Railway Administration of the People's Republic of China, Beijing, China

Wang FX (2014) Numerical simulation and vibrational characteristic analysis of high-speed railway due to environmental vibrations based on ABAQUS. MSc Thesis, Beijing Jiaotong University, Beijing, China (in Chinese)

Wang J, Liu X, Jiang Y, Chen J, Chen Q, Jiang S, Zhou N (2017) Critical distance between copper mining roadway and a vertical water-blocked body. *Quarterly Journal of Engineering Geology and Hydrogeology* 50(4):460-471, DOI: 10.1144/qjegh2016-122

Wang P, Wang J, Ma X, Ma D, Xu J, Qian Y (2018) Theoretical 3D model for quasistatic critical derailment coefficient of railway vehicles and a simplified formula. *Mathematical Problems in Engineering* 2018:7910753, DOI: 10.1155/2018/7910753

Xiao G (2019) Problems of railway tunnel construction under some special geological conditions in China and their countermeasures. *Tunnel Construction* 39(11):1748-1758, DOI: 10.3973/j.issn.2096-4498.2019.11.002 (in Chinese)

Xiao H, Li H, Tang Y (2018) Assessing the effects of rainfall, groundwater downward leakage, and groundwater head differences on the development of cover-collapse and cover-suffosion sinkholes in central Florida (USA). *Science of the Total Environment* 644:274-286, DOI: 10.1016/j.scitotenv.2018.06.273

Xu J, He J, Zhang L (2017) Collapse prediction of karst sinkhole via distributed Brillouin optical fiber sensor. *Measurement* 100:68-71, DOI: 10.1016/j.measurement.2016.12.046

Xu L, Zhang Q, Yu Z, Zhu Z (2020) Vehicle–track interaction with consideration of rail irregularities at three-dimensional space. *Journal of Vibration & Control* 26(92):1077, DOI: 10.1177/1077546319894816

Zhao YY, Ling XZ, Wang ZY, Shao XY, Tian LH, Geng L (2015) Test on dynamic characteristics of subgrade of heavy-haul railway in cold regions. *Sciences in Cold and Arid Regions* 7(005):605-610

Zhong S, Sun H, Li S, Li X, Wang R (2012) Detection and forecasting for hidden danger of karst fissure water and other geological disasters during construction of tunnels and underground projects. *Chinese Journal of Rock Mechanics and Engineering* 31:3298-3327, DOI: 10.3969/j.issn.1000-6915.2012.z1.095 (in Chinese)

Zhou Q, Chen L, Singh VP, Zhou J, Chen X, Xiong L (2019) Rainfall-runoff simulation in karst dominated areas based on a coupled conceptual hydrological model. *Journal of Hydrology* 573:524-533, DOI: 10.1016/j.jhydrol.2019.03.099